

REPORT



Protein engineering to increase the potential of a therapeutic antibody Fab for long-acting delivery to the eye

Devin Tesar^a, Jacob Luoma^a, Emily A. Wyatt^{a,†}, Catherine Shi^a, Whitney Shatz^b, Philip E. Hass^b, Mary Mathieu^c, Li Yi^d, Jacob E. Corn^{e,†}, Katie F. Maass^f, Kathryn Wang^a, Michelle Z. Dion^a, Nisana Andersen^g, Kelly M. Loyet^h, Menno van Lookeren Campagneⁱ, Karthikan Rajagopal^a, Leslie Dickmann^f, Justin M. Scheer^{b,†}, and Robert F. Kelley^a

^aDepartments of Drug Delivery, South San Francisco, CA; ^bDepartments of Protein Chemistry, South San Francisco, CA; ^cDepartments of Antibody Engineering, South San Francisco, CA; ^dDepartments of Pharmaceutical Development, South San Francisco, CA; ^eDepartments of Early Discovery Biochemistry, South San Francisco, CA; ^fDepartments of Clinical Pharmacology, South San Francisco, CA; ^gDepartments of Protein Analytical Chemistry, South San Francisco, CA; ^hDepartments of Biochemical and Cellular Pharmacology, South San Francisco, CA; ⁱDepartments of Immunology, Genentech Inc., 1 DNA Way, South San Francisco, CA

ABSTRACT

To date, ocular antibody therapies for the treatment of retinal diseases rely on injection of the drug into the vitreous chamber of the eye. Given the burden for patients undergoing this procedure, less frequent dosing through the use of long-acting delivery (LAD) technologies is highly desirable. These technologies usually require a highly concentrated formulation and the antibody must be stable against extended exposure to physiological conditions. Here we have increased the potential of a therapeutic antibody antigen-binding fragment (Fab) for LAD by using protein engineering to enhance the chemical and physical stability of the molecule. Structure-guided amino acid substitutions in a negatively charged complementarity determining region (CDR-L1) of an anti-factor D (AFD) Fab resulted in increased chemical stability and solubility. A variant of AFD (AFD.v8), which combines light chain substitutions (VL-D28S:D30E:D31S) with a substitution (VH-D61E) to stabilize a heavy chain isomerization site, retained complement factor D binding and inhibition potency and has properties suitable for LAD. This variant was amenable to high protein concentration (>250 mg/mL), low ionic strength formulation suitable for intravitreal injection. AFD.v8 had acceptable pharmacokinetic (PK) properties upon intravitreal injection in rabbits, and improved stability under both formulation and physiological conditions. Simulations of expected human PK behavior indicated greater exposure with a 25-mg dose enabled by the increased solubility of AFD.v8.

ARTICLE HISTORY

Received 11 July 2017
Revised 18 August 2017
Accepted 21 August 2017

KEYWORDS

age-related macular degeneration; isomerization; deamidation; stability; solubility; protein engineering; high concentration formulation; long-acting delivery



Introduction

Age-related macular degeneration (AMD) is a progressive chronic disease of the central retina with significant consequences for visual acuity.¹ Advanced forms of the disease include neovascular AMD and geographic atrophy (GA). Neovascular AMD is a leading cause of blindness in the Western world. It is characterized by excessive growth of blood vessels from the choroid behind the retina, and can cause severe visual impairment. Visual acuity for patients afflicted with neovascular AMD is often improved by treatment with anti-vascular endothelial growth factor (VEGF) agents such as Lucentis[®] (ranibizumab).^{2,3} GA is characterized by a progressive loss of photoreceptors and retinal pigment epithelial cells, leading to significant visual function impairment and eventual blindness. Even though GA affects more than 5 million people worldwide,⁴ there are currently no approved or effective treatment options for GA.

Although the molecular mechanism leading to GA is not well understood, studies suggest a link to polymorphisms in genes of

the alternative complement pathway.⁵ Complement factor D (CFD),⁶ a serine protease, catalyzes the cleavage and activation of factor B, which is a key step in the alternative complement cascade. It is thus an attractive target for intervention in GA.⁷ Lampalizumab is a humanized anti-factor D antigen-binding fragment (AFD) that binds to an exosite on CFD⁸ and potently inhibits its activity. Lampalizumab has shown efficacy in the treatment of GA through monthly 10-mg intravitreal dosing⁹ and has been advanced to pivotal clinical trials.

Monthly intravitreal drug administration may be burdensome to some patients, and less frequent dosing would be desirable. An increase in the amount dosed could result in improved treatment interval; however, the limited solubility of AFD at low ionic strength poses challenges for ocular formulations. Solubility can be increased with higher ionic strength, but hypertonic formulations are associated with an increased risk for retinal edema and detachment.¹⁰ Additional challenges include the small (~100 μ L) maximum volume acceptable for

CONTACT Robert F. Kelley  rk@gene.com  Genentech, Inc., 1 DNA Way, South San Francisco, CA 94080

 Supplemental data for this article can be accessed on the [publisher's website](#).

[†]Current address: Emily A. Wyatt, Chemical Engineering, Caltech; Jacob E. Corn, Innovative Genomics Institute, UC-Berkeley; Justin M. Scheer, Boehringer Ingelheim, Danbury, CT.

© 2017 Devin Tesar, Jacob Luoma, Emily A. Wyatt, Catherine Shi, Whitney Shatz, Philip E. Hass, Mary Mathieu, Li Yi, Jacob E. Corn, Katie F. Maass, Kathryn Wang, Michelle Z. Dion, Nisana Andersen, Kelly M. Loyet, Menno van Lookeren Campagne, Karthikan Rajagopal, Leslie Dickmann, Justin M. Scheer, and Robert F. Kelley. Published with license by Taylor & Francis Group, LLC This is an Open Access article distributed under the terms of the Creative Commons Attribution-NonCommercial-NoDerivatives License (<http://creativecommons.org/licenses/by-nc-nd/4.0/>), which permits non-commercial re-use, distribution, and reproduction in any medium, provided the original work is properly cited, and is not altered, transformed, or built upon in any way.

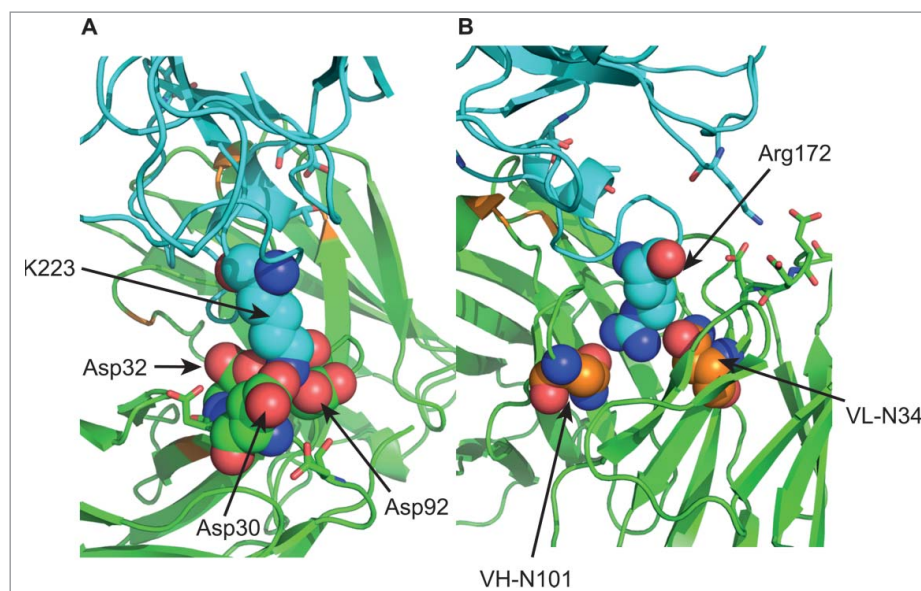


Figure 1. Key contacts observed in structure of AFD:CFD complex (4D9R). AFD and CFD are shown as green and aqua ribbons, respectively. Residues in contact with (A) CFD-Lys223 or (B) CFD-Arg172 are shown in space-filling and numbered. Figure prepared using Pymol (Schrödinger).

intravitreal injections, and the ocular clearance rate of antibodies ($t_{1/2} = 9.8$ days for bevacizumab²⁶) and antibody Fabs ($t_{1/2} = 5.9$ days for lampalizumab,^{11,12} 7.2¹³–8.6¹⁴ days for ranibizumab) relative to the desired treatment interval.

Sustained-release formulations or engineering of proteins to extend their half-life could facilitate an extended dosing interval for ocular therapeutics.¹⁵ Both approaches for antibody treatment of back-of-the-eye disorders may require highly concentrated formulations and high antibody stability under physiological conditions. Here, we describe the improved solubility and physical and chemical stability of AFD obtained through amino acid changes in the complementarity-determining region (CDR), creating a potential therapeutic that is amenable to long-acting delivery.

Results

Protein engineering of AFD

The CDR-L1 of AFD (²⁴I-T-S-T-D-I-D-D-D-M-N³⁴) provides a critical contact for the binding of CFD.⁸ Asp-30 and Asp-32, together with Asp-92 from CDR-L3, form an ionic interaction with Lys-223 of CFD (Figure 1A). Asp-30 is part of a “DD” motif and undergoes rapid isomerization to the cyclic intermediate form that is stable and elutes as a basic peak upon ion-exchange chromatography.^{16,17} This basic species showed a modest decrease, about 2-fold, in CFD-binding affinity (Supplemental Figure 1). Examination of the structure of the complex formed between CFD and AFD suggested that replacement of Asp-30 with less isomerization-prone Glu might preserve binding. AFD has a high affinity for CFD, as indicated by $K_D \sim 10$ pM, which is the limit that can be determined with surface plasmon resonance (SPR) technology. Thus, variants with $K_D \leq 10$ pM are considered equivalent to AFD. Within this constraint, the D30E mutant (variant AFD.v2) retained high affinity for CFD (Table 1).

AFD showed reduced solubility at pH 6 and low ionic strength (Figure 2), which was reversed through the addition of salt. Results of molecular docking simulations (Figure 3A) suggested that basic and acidic patches on AFD interact to stitch together Fabs in repeating units that support extended structures. We tested whether the acidic CDR-L1 was involved in these structures by replacing negatively charged residues in this region with Ser. Aspartic acid residues 28 and 31 in CDR-L1 are not in direct contact with CFD and individual substitution of these residues with Ser (variants AFD.v1 and AFD.v3, respectively) did not have any apparent effect on affinity for CFD (Table 1). In contrast, replacement of Asp32 with Ser (variant AFD.v4) resulted in a significant loss in CFD binding. Binding loss also occurred when this substitution was combined with the D28S and D31S mutants (variant AFD.v5). The CFD binding affinity for variant AFD.v6, which combined VL-

Table 1. Effect of amino acid changes on affinity for CFD determined using surface plasmon resonance.

Variant	Amino Acid Substitutions	K_D (pM)
AFD	NA	≤ 10
AFD.v1	VL-D28S	≤ 10
AFD.v2	VL-D30E	≤ 10
AFD.v3	VL-D31S	≤ 10
AFD.v4	VL-D32S	26
AFD.v5	VL-D28S:D31S:D32S	280
AFD.v6	VL-D30E:D31S VH-D61E	≤ 10
AFD.v7	VL-D30E:D31S:D92E VH-D61E	≤ 10
AFD.v8	VL-D28S:D30E:D31S VH-D61E	16.7 ± 4.4
AFD.v9	VL-D28S:D30E:D31S:N34S VH-D61E	30
AFD.v10	VL-D28S:D30E:D31S:D92E VH-D61E	70
AFD.v11	VL-D28S:D30E:D31S VH-N52S:D61E	70
AFD.v12	VL-D28S:D30E:D31S VH-D61E:N101D	23
AFD.v13	VL-D28S:D30E:D31S VH-D61E:N101Q	60
AFD.v14	VL-D28S:D30E:D31S VH-D61E:N101S	25.6 ± 6.3

Mutants are named based on location in light chain variable domain (VL) or heavy chain variable domain (VH): single letter code for the wild-type residue followed by sequence position (Kabat numbering scheme) followed by single letter code for the substituted amino acid. Multiple changes on the same domain are separated by a colon.

Molecule	Isoelectric point (pI)	Concentration before dialysis (mg/mL)	Concentration after precipitate measured at 4°C (mg/mL)
AFD	7.8	102	40
AFD.v2	ND	102	14
AFD.v6	8.0	102	92
AFD.v8	8.0	100	94
AFD.v14	8.0	103	47

Figure 2. Solubility of AFD molecules in 20 mM His-HCl, pH 6.0. Protein concentration in supernatant following centrifugation was determined by UV absorbance measurements. Photograph shows precipitate obtained upon centrifugation of the dialyzed sample.

D30E, D31S, and VH-D61E, was equivalent to that for AFD. The VH-D61E substitution eliminated an isomerization site that is not in contact with CFD and the substitution did not perturb CFD binding. Variant AFD.v8, which was generated by combining substitutions VL-D28S, D30E, D31S, and VH-D61E, had only a small (~2-fold) loss in affinity for CFD. The Asp to Ser substitutions altered the surface patch of negative charge contributed by CDR-L1 (Figure 3B).

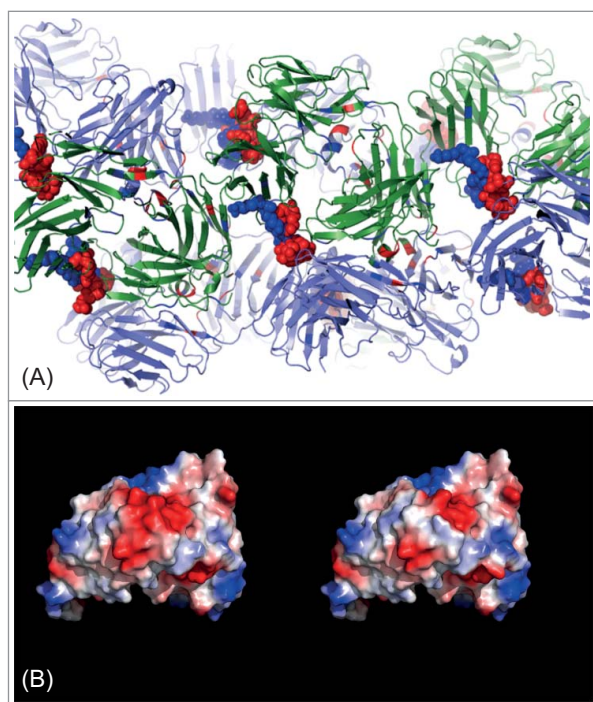


Figure 3. Self-association and molecular charge of AFD. (A) One potential cluster from molecular docking simulations of AFD self-association. (B) Electrostatic surface modeled for AFD (left) and AFD.v8 (right). Surfaces calculated and displayed using Pymol (Schrödinger) and AFD coordinates from AFD:fd complex structure (pdb code: 4D9R). AFD.v8 substitutions were modeled onto 4D9R structure.

Solubility measurements on AFD and AFD variants

The solubility of AFD, AFD.v2, AFD.v6, and AFD.v8 at pH 6 and under low ionic strength was compared. Solutions of AFD and AFD.v2 (~100 mg/mL in 20 mM His-HCl, pH 6) were noticeably turbid; a large pellet formed upon centrifugation, and there was a significant decrease in the protein concentration in the supernatant (Figure 2). The solution of AFD.v6 was less turbid, with a smaller precipitate formed upon centrifugation and a higher protein concentration in the supernatant. No precipitate was observed for AFD.v8, with the protein concentration in the supernatant consistent with full solubility of the Fab under these conditions. Variants AFD.v6 and AFD.v8 have 1 and 2 fewer negatively charged residues, respectively, than AFD; however, these changes did not produce a significant change in isoelectric point (pI).

Since long-acting delivery will involve extended exposure of an antibody Fab to neutral pH, which favors deamidation, we tested the effect of substituting potential sites of deamidation in the CDRs with other residues. For Asn residues in contact with CFD in the co-crystal structure (VL-N34, VH-N52, VH-N101; Figure 1B) only Asn-101 showed a significant rate of deamidation under neutral pH conditions. Results of peptide mapping showed that the extent of deamidation at Asn-101 increased by 11% for a 10-mg/mL sample of AFD.v6 when incubated in 10 mM phosphate buffer, pH 7.4 for 10 weeks at 37°C. Substitution of Asn-101 with Asp or Ser resulted in small losses in affinity for CFD (Table 1). As shown in Table 2, AFD and variants AFD.v7, AFD.v8, and AFD.v14 were equipotent with respect to

Table 2. Potency in CFD inhibition assay.

Variant	IC50 (nM) AP Hemolysis	IC50 (pM) fB activation
AFD	3.4	43
AFD.v7	3.8	50
AFD.v8	4.2	45
AFD.v14	4.1	51

inhibition of CFD enzymatic activity, as determined using a hemolysis assay and an assay of CFD-dependent factor B activation.

As shown in Figure 2, variant AFD.v14 was less soluble than AFD.v8 at pH 6, low ionic strength conditions. However, the solubility of AFD.v14 increased from 47 mg/mL to 80 mg/mL when the samples were incubated overnight at 37°C prior to centrifugation. In addition, AFD.v8 and AFD.v14 show high solubility at physiological pH and ionic strength. At the highest protein concentrations tested for solubility in phosphate-buffered saline (PBS), clear solutions of AFD.v8 (269 mg/mL) and AFD.v14 (372 mg/mL) were obtained. On the other hand, precipitation was observed for AFD, which had a maximum solubility of 227 mg/mL in PBS.

Assessment on chemical and physical stability of AFD variants

To further compare the suitability of variants AFD.v8 and AFD.v14 as candidate therapeutic agents, we performed stability studies at a concentration of 100 mg/mL Fab in PBS. The conditions simulated those expected during extended exposure to physiological conditions in a long-acting delivery system. Both AFD.v8 and AFD.v14 retained antigen-binding capacity upon incubation in PBS at 37°C for at least 10 weeks (Figure 4). The loss in binding capacity at 10 weeks as determined using SPR was less than the standard error ($\pm 10\%$) in the measurements. In contrast, the binding capacity of AFD decreased by $\sim 30\%$ at 10 weeks. Both variants showed a low tendency to aggregate under this stress condition (Supplemental Figure 2) and basic peak formation was absent (Supplemental Figure 3). The rate of acidic variant generation for AFD.v14, which has the additional VH-N101S change, was negligible, suggesting that deamidation of VH-Asn101 accounted for the acidic species production in AFD. AFD.v8 showed good stability in a formulation with high concentration and low ionic strength, pH

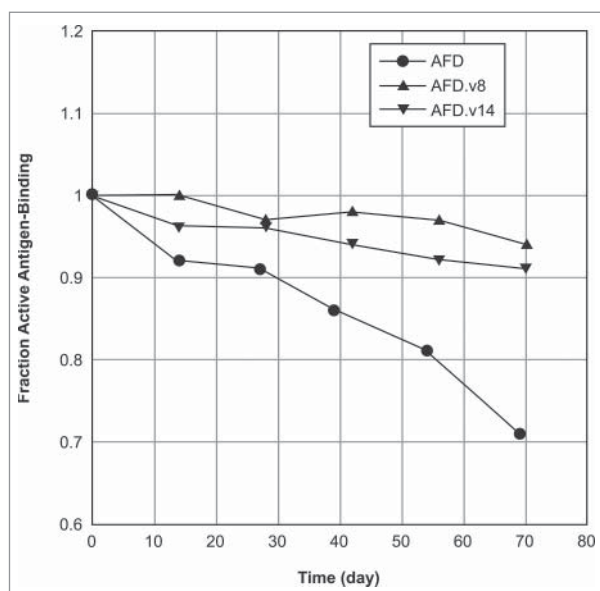


Figure 4. Fraction of antibody Fab active for antigen binding as determined using SPR. Protein solutions (100 mg/mL in PBS) were incubated at 37°C for various times.

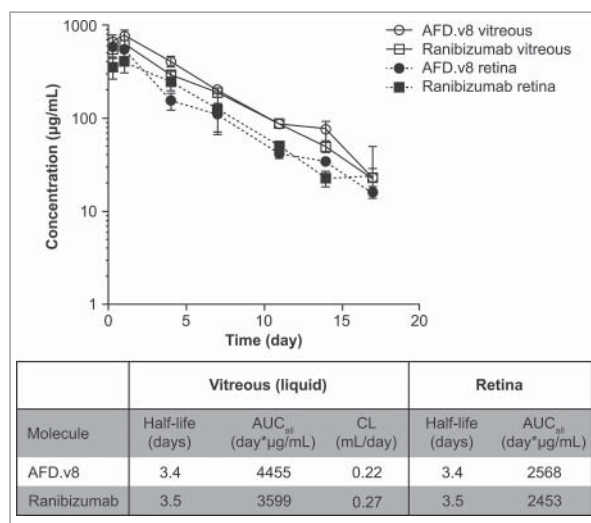


Figure 5. Concentration-time profile observed for ranibizumab and AFD.v8 following intravitreal injection (1.0 mg/eye) in rabbits. Concentrations in vitreous humor and retina were determined by ELISA. Pharmacokinetic parameters derived from a noncompartmental analysis are shown in the inset.

5.5 (Supplemental Figures 4–5). At a concentration of 272 mg/mL and pH 5.5, AFD.v8 retained $>80\%$ of antigen-binding capacity after a 4-month incubation at 37°C (Supplemental Figure 4). Loss of binding observed at 8 months likely resulted from a decrease in monomer content, deamidation of CDR-H3 Asn-101 (17%), and isomerization of CDR-H3 Glu-95 (5%) (Supplemental Figure 5).

Pharmacokinetic studies and simulations of AFD.v8

Given the improved stability and solubility of AFD.v8, *in vivo* rabbit studies were conducted with this variant. AFD and variants do not bind rabbit CFD, therefore, pharmacokinetic (PK) experiments in rabbits provide a measure of target-independent clearance from ocular tissue. Vitreous humor concentration-time curves obtained following intravitreal injection of 1.0 mg AFD.v8, or a comparator dose of ranibizumab, are shown in Figure 5. Analysis of the data using a non-compartmental approach indicated that clearance of AFD.v8 and ranibizumab is comparable. PK parameters calculated for ranibizumab are consistent with results of earlier studies in rabbits.¹⁸ Both antibody Fabs showed similar exposure levels in the retina. The amino acid changes in AFD.v8, which improved solubility and stability compared to AFD, did not have a deleterious consequence for ocular PK.

We simulated human PK upon intravitreal injection of AFD.v8 based on the assumption that this variant would have PK similar to lampalizumab. The previously published lampalizumab population PK model¹² was used with the PK parameters estimated for lampalizumab. In Figure 6, simulated vitreous concentrations for AFD.v8 are shown for 2 doses, a 10-mg dose – equivalent to that used in the lampalizumab Phase 2/3 clinical trials – and a 2.5-fold higher dose of 25 mg. The higher dose afforded by the increased solubility of AFD.v8 results in higher vitreous drug concentrations, and thus higher drug exposures compared with the 10-mg dose when given at the same treatment frequency. A higher dose may potentially enable less frequent dosing with similar efficacy outcomes. In Table 3, the drug concentrations and exposures for 5 dose regimens are

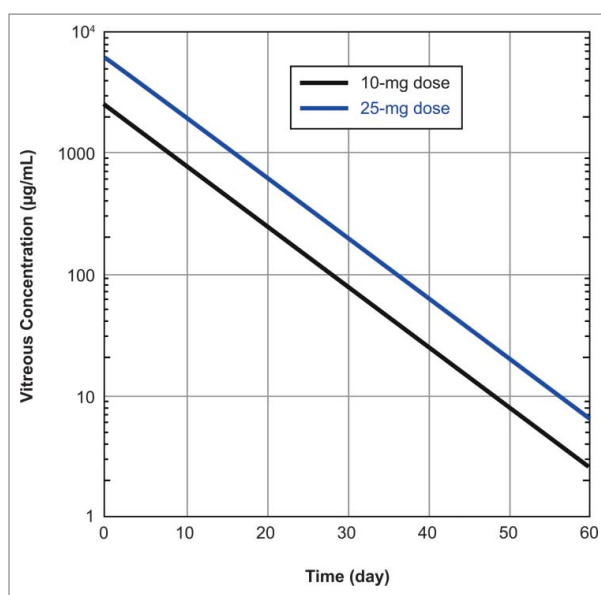


Figure 6. Simulated human vitreous concentration-time profiles for 10- and 25-mg doses. Simulations are based on the previously published population pharmacokinetic model for lampalizumab.¹² The 10-mg and 25-mg dose lines represent predictions for a typical patient.

compared: 10-mg dose every 4 weeks (Q4W), 10-mg dose every 6 weeks (Q6W), 25-mg dose Q4W, 25-mg dose Q6W, and 25-mg dose every 8 weeks (Q8W). The total area under the concentration-time curve over the course of a 72-week treatment period ($AUC_{[0-72wk]}$) is increased for all dosing regimens of the higher dose relative to 10 mg Q4W, including 25 mg Q8W. None of the dosing schemes summarized in Table 3 result in accumulation of drug since the minimum drug concentration between doses (C_{min}) does not change appreciably with repeat dosing. Higher C_{min} is observed with 25 mg Q4W than with 10 mg Q4W, but is lower for less frequent administration (Q6W and Q8W) of a 25-mg dose.

Discussion

Results of analysis on AFD samples exposed to vitreous humor conditions (data not shown) suggest that this molecule has sufficient *in vivo* stability to support an increased dosing interval. The variants described here have improved solubility that facilitated higher concentration formulations. The decreased solubility of AFD observed at pH 6 and low ionic strength is thought to reflect weak intermolecular electrostatic interactions that drive assembly into higher-order structures. CDR-L1 appears to form at least a portion of an acidic patch that is involved in this electrostatic interaction since Asp to Ser amino acid changes in this region (VL-D28S, D31S) resulted in improved solubility. In

contrast to this charge-mediated interaction, hydrophobic to hydrophilic substitutions in the variable domains of a bispecific IgG antibody were required to improve solubility.¹⁹ The specific distribution of charge on AFD appears to be at least as important as total charge in determining the solubility properties of the molecule since the replacements in CDR-L1 did not produce a large change in pI. The small change in pI may reflect altered pKa values for some of the Asp residues in CDR-L1 of AFD such that the pKa of the remaining residues became normalized when Asp-28 and Asp-31 were replaced with Ser. Indeed, the high isomerization rate of Asp-30 is consistent with an atypical, high pKa for this residue²⁰ because the protonated side chain favors formation of the cyclic imide that is the intermediate for isomerization. Interestingly, the highly negatively charged CDR-L1 of AFD is encoded in the mouse germline gene. AFD also conserves positively charged regions with the variable domains of the parental murine antibody, suggesting that the solubility behavior observed in low ionic strength conditions is not a consequence of the grafting of mouse CDRs into a human framework.

The challenge of engineering improved solubility is shown by the apparent lowering of solubility (pH 6.0, low ionic strength) upon introduction of the VH-N101S substitution. Variants AFD.v8 and AFD.v14 differ by this change, but otherwise have the same pI and calculated net charge at pH 6.0. In addition to forming contacts with antigen in the CFD-bound structure of AFD, Asn-101 also appears to make hydrogen-bonding interactions with other residues of CDR-H3. Modeling indicates a Ser residue could not make equivalent interactions, suggesting that the conformation of CDR-H3 is de-stabilized in AFD.v14, which has consequences for solubility at pH 6.0 and low ionic strength. Therefore, in choosing a candidate for long-acting delivery, the incremental increase in chemical stability for AFD.v14 compared to AFD.v8 must be balanced by a consideration of their solubility differences, and the slightly weaker (<2-fold) affinity of AFD.v14 for CFD.

The stability of both AFD.v8 and AFD.v14, as indicated by the full retention of antigen-binding capacity for at least 10 weeks in 37°C PBS, renders both suitable for long-acting delivery to the eye (Figure 4). Charge variant generation was negligible for AFD.v14, whereas an appreciable rate of acidic species production, likely attributed to VH-N101 deamidation, was observed for AFD.v8. The additional benefit of the VH-N101S substitution to preservation of antigen-binding was not realized in this experiment. This is not surprising because, although the acidic peak accumulated to ~25% under these stress conditions, the effect of a negatively charged residue at this position (Asp in AFD.v12) on binding affinity was small (<2-fold). A comparison of all variants suggests that amino acid changes VL-D28S and D30E improve retention of antigen-binding capacity for thermally stressed samples.

AFD.v8 is well adapted for high concentration (≥ 250 mg/mL) formulations as it showed low viscosity (Supplemental Figure 6) that facilitates intravitreal injection. Either a high concentration formulation, and hence higher dose, or a slow release formulation providing sustained exposure could enable an additional therapeutic option with less-frequent dosing for patients. Efficacy of AFD.v8 may be driven by total drug exposure, maintenance of drug concentrations above an efficacy threshold, or other PK characteristics. If total drug exposure

Table 3. Simulated human vitreous exposure levels and concentrations.

Dose scheme	$AUC_{[0-72wk]}$ (mg/mL*day)	Relative AUC	C_{min} (µg/mL)
10 mg Q4W	440	1	77
10 mg Q6W	293	0.67	11
25 mg Q4W	1142	2.5	207
25 mg Q6W	762	1.67	31
25 mg Q8W	572	1.25	5

drives efficacy, the 25-mg dose would be expected to have human vitreal exposure (Table 3) superior to the 10-mg Q4W dose over the course of treatment whether given Q4W, Q6W, or Q8W; however, the 10-mg Q4W dose would produce higher C_{\min} than 25-mg Q6W or Q8W and may be superior if maintenance of drug concentrations above an efficacy threshold is needed for efficacy and that threshold is passed with less frequent dosing. Further clarification of the relationship between PK and efficacy awaits the outcome of the pivotal trials of lampalizumab in GA. Nonetheless, a higher dose formulation has potential to bring further benefit to patients.

A relatively stable, highly concentrated (272 mg/mL) formulation with low ionic strength, pH 5.5, is achievable for AFD.v8, whereas the parental antibody, AFD, showed low solubility under this condition. Full antigen binding was maintained for at least 2 months at 37°C (Supplemental Figure 4), suggesting that a high concentration liquid formulation of AFD.v8 stored frozen or at 2–8°C is viable. However, elimination of the primary degradation mode of AFD, VL-Asp-30 isomerization, has revealed other, slower degradation processes, including isomerization of a glutamic acid residue. AFD has a short CDR-H3: ⁹⁵E-G-G-V-N-N¹⁰² (Kabat numbering). Since Glu-95 forms a key contact with CFD,⁸ isomerization of this residue, albeit at a very slow rate, could affect binding. Further engineering may be required to obtain a molecule with retention of full activity for ≥4 months upon thermal stress.

Therapeutic agents administered to the eye via intravitreal injection must be isotonic in order to minimize intraocular pressure changes and the potential for retinal edema and detachment.¹⁰ They should also be low in viscosity for ease of administration. Although increased salt concentration can prevent the electrostatic-mediated association we have described here for AFD, increased salt poses challenges to maintain the tonicity of the formulation. The alternative approach we have demonstrated is to mitigate the self-association through structure-based design of sequence variants with improved properties. This approach could be applied to other therapeutic antibodies that have similar limitations in solubility and stability, provided that sufficient information is available to design agents that retain potency and favorable PK properties. An anti-interleukin (IL)13 antibody was shown to have an aggregation-prone sequence in CDR-H3, but amino acid changes to improve solubility resulted in decreased IL13 binding, increased viscosity or tendency to aggregate.^{21,22} The most successful approach to increase solubility of the anti-IL13 antibody was to introduce a glycosylation site that could mask the aggregation-prone region with minimal effect on IL13 binding. Addition of a glycosylation site is not an option for production in *Escherichia coli*, which is used for ranibizumab and lampalizumab. Since we introduced amino acid changes only in the hypervariable regions of the antibody Fab, we expect these variants to have low risk for increased immunogenicity in humans.

Materials & methods

Materials

Purified human VEGF (1-165), human factor D (CFD), ranibizumab, and AFD were supplied by Genentech, Inc.

Methods

Mutant construction and Fab expression/purification

Mutations were introduced by site-directed mutagenesis using the QuikChangeII[®] site-directed mutagenesis kit (Agilent) following the manufacturer's instructions. Oligonucleotide primers specifying the required codon changes were synthesized by the Genentech oligonucleotide synthesis lab. Plasmids with designed changes were identified and confirmed by DNA sequencing at Genentech. For small scale-expression and purification, DNA was transformed into *Escherichia coli* strain 64B4, and the cells were grown overnight in low phosphate-containing media. The Fab was purified from cell lysates prepared using PopCulture[®] extraction buffer (EMD Millipore) through chromatography on Protein G GraviTrap (GE Healthcare). For larger scale purification, cell paste from 10 L fermentation of the transformed cells was provided by the Genentech fermentation group. Cell paste was suspended in extraction buffer and homogenized using a microfluidizer. Fabs were captured by immunoaffinity chromatography on Protein G-Sepharose and eluted with a low pH buffer. The low pH eluate was adjusted to pH 5.0 and further purified by cation exchange chromatography on an S-Sepharose column. Identities of the purified proteins were confirmed by mass spectroscopy and the pooled fractions were concentrated to ~ 10 mg/mL, and exchanged into PBS buffer via diafiltration.

Binding affinity by surface plasmon resonance measurements

Determination of the K_D for CFD binding to immobilized AFD was determined by SPR measurements on a Biacore[®] T200 instrument using a protocol similar to that described by Ultsch et al.²³ except that antibody Fabs were immobilized on a Series S CM5 sensor chip using the anti-huFab capture kit (GE healthcare Cat. # 28-9583-25) following the manufacturer's protocol. The running buffer was 10 mM HEPES pH 7.4, 150 mM NaCl, 0.01% PS20, the temperature of analysis was 25°C, and a flow rate of 30 μ L/min was used.

Alternative pathway hemolysis and factor B TR-FRET assays

Half-maximal inhibition (IC₅₀) values for inhibition of complement activation in an alternative pathway hemolysis assay were determined as described previously.²⁴

Factor B TR-FRET assay – Dilutions of AFD Fab or control were prepared in enzymatic reaction buffer (ERB; 75 mM NaCl, 1 mM MgCl₂, 25 mM Tris, 0.005% polysorbate 20, pH 7.3) at a 4x concentration and combined in equal volumes with 0.5 nM CFD (Complement Technology) or ERB (no enzyme control). The CFD/AFD mixtures (7 μ L/well) were added to 364-well Proxiplate F plus black plates (Perkin Elmer Health Sciences) followed by 7 μ L/well of substrate. The substrate consisted of a mixture of C3b (Complement Technology) at 7 μ g/mL (39.7 nM) and factor B (Complement Technology) at 1 μ g/mL (10.8 nM). The Fab, enzyme, cofactor, and substrate were incubated for 45 min at room temperature with gentle agitation. The reaction was stopped with 7 μ L/well of a detection reagent cocktail mixture consisting of 8 nM biotinylated anti-factor Bb (2F12, GNE PRO282909), 4 nM Europium-conjugated anti-factor Ba (custom conjugation of 1C3, GNE

PRO282908 by Life Technologies), and 25 nM streptavidin-Alexa 647. The plate was incubated at room temperature in the dark for 30 min. Time-resolved fluorescence energy transfer was detected with a PHERAstar FS microplate reader (BMG LabTech) by exciting at 337 nm and detecting Europium emission at 620 nm and Alexa fluor emission at 665 nm. The AFD concentrations causing IC₅₀ were determined by nonlinear regression analysis using a four-parameter fit model (Kaleida-Graph Synergy Software).

Solubility testing

Protein solutions formulated in 20 mM His-HCl, pH 5.0 were concentrated to 100 mg/mL using Amicon Centriprep YM-10 centrifugal filter units. Samples (0.5–1 mL) were placed in Slide-A-Lyzer cassettes with a molecular weight cutoff of 10 K (Pierce, Thermo Scientific) and dialyzed overnight at 4°C versus 1 L of 20 mM His buffer, pH 6.0. Samples were removed from the cassette, visually inspected for aggregates, centrifuged at 14,000 × g for 10 min to pellet any insoluble material, and the protein concentration in the supernatant was determined by UV absorbance measurements. A similar procedure was used for comparing solubility of variants under conditions of physiological pH and ionic strength except that the samples were concentrated to >200 mg/mL and dialyzed overnight at 4°C versus PBS.

Simulations on AFD self-association

Macromolecular docking was performed using HADDOCK²⁷ with restraints introduced between lysine and aspartate/glutamate residues derived from antibody crosslinking data (Li Yi, unpublished results). AFD docking utilized 279 restraints, while control antibody (ranibizumab) docking utilized 25 restraints. A total of 2000 rigid body trials were performed with each antibody complex, randomly excluding 50% of the restraints in each trial. Semi-flexible refinement was performed on the top 200 decoys for each complex and refined structures were clustered based on root mean square deviation. The top-scoring AFD cluster exhibited good convergence (59 decoys, rmsd 0.77 ± 0.49 Å).

Stability samples

Proteins were concentrated to ~ 10 mg/mL or 100 mg/mL using centrifugal filter units as described above. Samples were dialyzed against the buffer condition for test, PBSTN (10 mM sodium phosphate, 137 mM NaCl, pH 7.4 containing 0.02% polysorbate 20 and 0.02% sodium azide) or 10 mM His-HCl pH 5.5, or 20 mM His-HCl pH 5.5, and then adjusted to the final protein concentration by further centrifugal concentration or by dilution. Samples were incubated at 37°C. Aliquots were removed at various time points, diluted to 1 mg/mL with 10 mM His-HCl pH 5.5 10% trehalose, and snap frozen for storage at -80°C. CFD binding was determined as described below. Analysis for charge variation and monomer content is described in Supplemental Methods.

Binding capacity by SPR measurements

Functional activity for binding to immobilized CFD was assessed by SPR measurements on a Biacore[®] T200 instrument¹ (GE Healthcare) with CFD covalently immobilized on a

Series S, CM5 sensor chip using amine-coupling chemistry. Antigen-binding active concentrations of AFD were determined using the calibration-dependent concentration analysis routine of the Biacore[®] T200 evaluation software. A calibration curve of unstressed AFD, as well as samples of stressed material, were prepared through gravimetric dilution. All samples (200 μL volume) were prepared using 1X running buffer (10 mM HEPES pH 7.4, 150 mM NaCl, 0.01% PS20); 60-μL aliquots were injected over the specific antigen surface using a flow rate of 10 μL/min, and bound antibody Fab was determined from the SPR signal near the end of the sample injection. The sensor chip surface was regenerated between binding cycles through injection of 10 mM Gly-HCl, pH 2.1. The standard curve of starting material was used to determine the relationship of SPR signal to antibody concentration using a four-parameter function to analyze the data. Parameters calculated from the standard curve were used to calculate the antigen-binding concentration of test samples based on the observed SPR signal. The ratio of this concentration to the protein concentration determined by absorbance measurements gives the fraction or percent binding. This method was qualified with ±10% standard error using a recovery experiment.

ELISA assay of pharmacokinetic study samples

Analyses of AFD.v8 and ranibizumab were done using a generic immunoglobulin PK ELISA²⁵ as previously described with the following modifications. 384-well ELISA plates were blocked with PBS plus 0.5% bovine serum albumin (BSA) at room temperature. The samples, controls, and standard curves were prepared in sample assay diluent at pH 7.4; rabbit vitreous humor or retinal homogenate samples were diluted at a minimum of 1:100 or 1:50, respectively. Detection was with 83.3 ng/mL HRP-conjugated sheep anti-human IgG mAb (Bethyl Laboratories Inc) in conjugate assay diluent (PBS + 0.5% BSA + 0.05% Tween 20 + 10 ppm Proclin), followed by tetramethyl benzidine peroxidase substrate (Moss, Inc.). Assay sensitivities in rabbit vitreous or retinal homogenate were 62.5 ng/mL or 31 ng/mL, respectively.

Pharmacokinetic experiments and assay

Animal studies were conducted at Covance Laboratories (Madison, WI) in accordance with the Animal Welfare Act, the Guide for the Care and Use of Laboratory Animals, and the Office of Laboratory Animal Welfare.

Naïve New Zealand white rabbits (n = 24; male; >2.5 kg; aged 5–7 months at the time of dosing) were treated with AFD.v8 or ranibizumab via a single bilateral intravitreal injection and observed for up to 27 days.

Fabs were administered by a single 50-μL intravitreal injection (1.0-mg dose) to both eyes in all animals under sedation. Doses were administered by a board-certified veterinary ophthalmologist in accordance with Covance standard operating procedures (SOP).

All animals were euthanized in accordance with Covance SOP. At the time of euthanasia, both eyes were enucleated. Aqueous humor was collected fresh and then each eye was flash frozen in liquid nitrogen and stored at approximately -70°C. Within 2 days, the frozen vitreous and retina tissues were

collected separately as right and left eye. All tissues were kept at -70°C until analysis using the ELISA described above.

The following PK parameters were determined by noncompartmental analysis using the nominal time and dose (Phoenix WinNonlin, Pharsight Corp): C_{max} (maximum observed concentration); AUC_{all} (area under the vitreous concentration versus time curve from time 0 to C_{last}); CL (clearance calculated as nominal dose (mg/kg)/ AUC_{inf}); $t_{1/2, \text{elim}}$ (half-life associated with the terminal phase [$\ln(2)/\lambda_z$]) and V_{ss} (volume of distribution at steady-state).

Pharmacokinetic simulations

PK simulations were generated based on the previously published lampalizumab population PK model.¹² The PK parameters used in simulations are those parameters estimated for lampalizumab in the ocular-serum target-mediated drug disposition model for a typical patient.

Disclosure of potential conflicts of interest

All authors are current or former employees of Genentech, Inc., a member of the Roche group, and may own Roche stock or stock options.

Acknowledgments

The authors acknowledge helpful discussions with Atul Dandekar and Thierry Nivaggioli.

ORCID

Li Yi  <http://orcid.org/0000-0002-1994-0284>

Justin M. Scheer  <http://orcid.org/0000-0002-4621-2311>

References

1. Lim LS, Mitchell P, Seddon JM, Holz FG, Wong TY. Age-related macular degeneration. *Lancet*. 2012;379(9827):1728-1738. [https://doi.org/10.1016/S0140-6736\(12\)60282-7](https://doi.org/10.1016/S0140-6736(12)60282-7). PMID:22559899
2. Brown DM, Kaiser PK, Michels M, Soubrane G, Heier JS, Kim RY, Sy JP, Schneider S; ANCHOR Study Group. Ranibizumab versus verteporfin for neovascular age-related macular degeneration. *N Engl J Med*. 2006;355(14):1432-1444. <https://doi.org/10.1056/NEJMoa062655>. PMID:17021319
3. Rosenfeld PJ, Brown DM, Heier JS, Boyer DS, Kaiser PK, Chung CY, Kim RY; MARINA Study Group. Ranibizumab for neovascular age-related macular degeneration. *N Engl J Med*. 2006;355(14):1419-1431. <https://doi.org/10.1056/NEJMoa054481>. PMID:17021318
4. Wong WL, Su X, Li X, Cheung CM, Klein R, Cheng CY, Wong TY. Global prevalence of age-related macular degeneration and disease burden projection for 2020 and 2040: a systematic review and meta-analysis. *Lancet Glob Health*. 2014;2(2):e106-e116. [https://doi.org/10.1016/S2214-109X\(13\)70145-1](https://doi.org/10.1016/S2214-109X(13)70145-1). PMID:25104651
5. Yates JR, Sepp T, Matharu BK, Khan JC, Thurlby DA, Shahid H, Clayton DJ, Hayward C, Morgan J, Wright AF, et al. Genetic Factors in AMD Study Group. Complement C3 variant and the risk of age-related macular degeneration. *N Engl J Med*. 2007;357(6):553-561. <https://doi.org/10.1056/NEJMoa072618>. PMID:17634448
6. Volanakis JE, Narayana SV. Complement factor D, a novel serine protease. *Protein Sci*. 1996;5(4):553-564. <https://doi.org/10.1002/pro.5560050401>. PMID:8845746
7. Holz FG, Strauss EC, Schmitz-Valckenberg S, van Lookeren Campagne M. Geographic atrophy: clinical features and potential

- therapeutic approaches. *Ophthalmology*. 2014;121(5):1079-1091. <https://doi.org/10.1016/j.ophtha.2013.11.023>. PMID:24433969
8. Katschke KJ Jr., Wu P, Ganesan R, Kelley RF, Mathieu MA, Hass PE, Murray J, Kirchofer D, Wiesmann C, van Lookeren Campagne M. Inhibiting alternative pathway complement activation by targeting the factor D exosite. *J Biol Chem*. 2012;287(16):12886-12892. <https://doi.org/10.1074/jbc.M112.345082>. PMID:22362762
 9. Le K. Population PKPK modeling of geographic atrophy disease progression, target mediated disposition and treatment effect of lampalizumab. Population Approach Group. 2014;2014:II-07.
 10. Marmor MF, Martin LJ, Tharpe S. Osmotically induced retinal detachment in the rabbit and primate: electron microscopy of the pigment epithelium. *Invest Ophthalmol Vis Sci*. 1980;19(9):1016-1029. PMID:7409995
 11. Do DV, Pieramici DJ, van Lookeren Campagne M, Beres T, Friesenhahn M, Zhang Y, Strauss EC; Phase Ia Investigators. A phase Ia dose-escalation study of the anti-factor D monoclonal antibody fragment FCFD4514S in patients with geographic atrophy. *Retina*. 2014;34(2):313-320. <https://doi.org/10.1097/IAE.0b013e3182979ddd>. PMID:23842100
 12. Le KN, Gibiansky L, van Lookeren Campagne M, Good J, Davançaze T, Loyet KM, Morimoto A, Strauss EC, Jin JY. Population pharmacokinetics and pharmacodynamics of lampalizumab administered intravitreally to patients with geographic atrophy. *CPT Pharmacometrics Syst Pharmacol*. 2015;4(10):595-604. <https://doi.org/10.1002/psp4.12031>. PMID:26535160
 13. Krohne TU, Liu Z, Holz FG, Meyer CH. Intraocular pharmacokinetics of ranibizumab following a single intravitreal injection in humans. *Am J Ophthalmol*. 2012;154(4):682-686 e2. <https://doi.org/10.1016/j.ajo.2012.03.047>. PMID:22818800
 14. Xu L, Lu T, Tuomi L, Jumbe N, Lu J, Eppler S, Kuebler P, Damico-Beyer LA, Joshi A. Pharmacokinetics of ranibizumab in patients with neovascular age-related macular degeneration: a population approach. *Invest Ophthalmol Vis Sci*. 2013;54(3):1616-1624. <https://doi.org/10.1167/iovs.12-10260>. PMID:23361508
 15. Short BG. Safety evaluation of ocular drug delivery formulations: techniques and practical considerations. *Toxicol Pathol*. 2008;36(1):49-62. <https://doi.org/10.1177/0192623307310955>. PMID:18337221
 16. Zhang J, Yip H, Katta V. Identification of isomerization and racemization of aspartate in the Asp-Asp motifs of a therapeutic protein. *Anal Biochem*. 2011;410(2):234-243. doi: 10.1016/j.ab.2010.11.040. <https://doi.org/10.1016/j.ab.2010.11.040>. PMID:21130067
 17. Yi L, Beckley N, Gikanga B, Zhang J, Wang YJ, Chih HW, Sharma VK. Isomerization of Asp-Asp motif in model peptides and a monoclonal antibody Fab fragment. *J Pharm Sci*. 2013;102(3):947-959. <https://doi.org/10.1002/jps.23423>. PMID:23280575
 18. Gaudreault J, Fei D, Beyer JC, Ryan A, Rangell L, Shiu V, Damico LA. Pharmacokinetics and retinal distribution of ranibizumab, a humanized antibody fragment directed against VEGF-A, following intravitreal administration in rabbits. *Retina*. 2007;27(9):1260-1266. <https://doi.org/10.1097/IAE.0b013e318134eecc>. PMID:18046235
 19. Sampei Z, Igawa T, Soeda T, Okuyama-Nishida Y, Moriyama C, Wakabayashi T, Tanaka E, Muto A, Kojima T, Kitazawa T, et al. Identification and multidimensional optimization of an asymmetric bispecific IgG antibody mimicking the function of factor VIII cofactor activity. *PLoS One*. 2013;8(2):e57479. <https://doi.org/10.1371/journal.pone.0057479>. PMID:23468998
 20. Wakankar AA, Liu J, Vandervelde D, Wang YJ, Shire SJ, Borchardt RT. The effect of cosolutes on the isomerization of aspartic acid residues and conformational stability in a monoclonal antibody. *J Pharm Sci*. 2007;96(7):1708-1718. <https://doi.org/10.1002/jps.20823>. PMID:17238195
 21. Bethea D, Wu SJ, Luo J, Hyun L, Lacy ER, Teplyakov A, Jacobs SA, O'Neil KT, Gilliland GL, Feng Y. Mechanisms of self-association of a human monoclonal antibody CNTO607. *Protein Eng Des Sel*. 2012;25(10):531-537. <https://doi.org/10.1093/protein/gzs047>. PMID:22915597
 22. Wu SJ, Luo J, O'Neil KT, Kang J, Lacy ER, Canziani G, Baker A, Huang M, Tang QM, Raju TS, et al. Structure-based engineering of a monoclonal antibody for improved solubility. *Protein Eng Des Sel*. 2010;23(8):643-651. <https://doi.org/10.1093/protein/gzq037>. PMID:20543007

23. Ultsch M, Bevers J, Nakamura G, Vandlen R, Kelley RF, Wu LC, Eigenbrot C. Structural basis of signaling blockade by anti-IL-13 antibody Lebrikizumab. *J Mol Biol.* 2013;425(8):1330-1339. <https://doi.org/10.1016/j.jmb.2013.01.024>. PMID:23357170
24. Katschke KJ Jr., Stawicki S, Yin J, Steffek M, Xi H, Sturgeon L, Hass PE, Loyet KM, Deforge L, Wu Y, et al. Structural and functional analysis of a C3b-specific antibody that selectively inhibits the alternative pathway of complement. *J Biol Chem.* 2009;284(16):10473-10479.
25. Yang J, Ng C, Lowman H, Chestnut R, Schofield C, Sandlund B, Ernst J, Bennett G, Quarmby V. Quantitative determination of humanized monoclonal antibody rhuMAb2H7 in cynomolgus monkey serum using a Generic Immunoglobulin Pharmacokinetic (GRIP) assay. *J Immunol Methods.* 2008;335(1-2):8-20. <https://doi.org/10.1074/jbc.M809106200>, <https://doi.org/10.1016/j.jim.2008.01.016>. PMID:19196712. PMID:18402977
26. Krohne TU, Eter N, Holz FG, Meyer CH. Intraocular pharmacokinetics of bevacizumab after a single intravitreal injection in humans. *Am J Ophthalmol.* 2008; 146:508-512. <https://doi.org/10.1016/j.ajo.2008.05.036>. PMID:18635152
27. Dominguez C, Boelens R, Bonvin AM. HADDOCK: a protein-protein docking approach based on biochemical or biophysical information. *J Am Chem Soc.* 2003; 125:1731-1737. <https://doi.org/10.1021/ja026939x>. PMID:12580598